EPR Investigation of the Electronic Structure of Mononuclear Copper(I) Nitric Oxide Adduct Formed upon Low-Pressure Adsorption of NO onto Cu/ZSM-5 Zeolite

Zbigniew Sojka*,† and Michel Che‡

Laboratoire de Réactivité de Surface, URA 1106 CNRS, Université P. et M. Curie, 4 Place Jussieu, 75232 PARIS Cedex-05, France

Elio Giamello

Dipartimento di Chimica Inorganica, Chimica Fisica e Chimica dei Materiali, Universitá di Torino, Via P. Giuria 7, 10125 Torino, Italy

Received: February 24, 1997[⊗]

The adsorption of NO onto copper-exchanged ZSM-5 zeolite has been studied by EPR spectroscopy. A distinct Cu^+-NO species possessing an end-on η^1 bent structure has been identified. Its EPR spectrum with a well-defined superhyperfine coupling with $^{63,65}Cu$ nuclei and hyperfine coupling with ^{14}N was interpreted in terms of completely anisotropic **g** and hyperfine tensors with noncoincident axes (monoclinic symmetry). The spin Hamiltonian parameters of this adduct have been analyzed in detail, leading to a semiquantitative molecular orbital correlation picture of the complex. The model developed shows that the unpaired electron resides mainly on the angularly coordinated NO and the copper superhyperfine structure arises from delocalization of the unpaired electron density onto Cu a′ orbitals ($3d_{z^2}$, $3d_{xz}$, and 4s). The total spin density on copper is found to be equal to 0.2 and is shared among $3d_{z^2}$ (0.079), $3d_{xz}$ (0.021), and 4s (0.1) orbitals. The remaining part of the unpaired electron density is localized on nitrogen (0.55) and oxygen (0.25) atoms. The bonding interaction involves essentially an overlap of Cu $3d_{z^2}$ and $3d_{xz}$ with an antibonding 2p π* and a lone pair n orbital of the NO ligand as well as a $3d_{yz}$ overlap with a second orthogonal NO 2p π* orbital. The appropriate molecular orbital diagram has been devised to account for the EPR data. The model is consistent with the observed magnetic properties of the investigated adducts and satisfactorily explains the previously unrecognized complex source of hyperfine couplings. The implications of this coordination mode on the possible molecular mechanism of the catalytic decomposition of NO over Cu/ZSM-5 catalysts are discussed.

Introduction

Interaction of nitric oxide with transition metal ions (TMI) is a topic of great interest for several branches of chemistry.[1−10] Thus, in particular, understanding the mode of coordination of the nitric oxide and its activation by TMI is essential for unraveling the pathways of the catalytic reduction and conversion of NO in inorganic and biological nitrogen cycles.[1,5−11]

Metal nitrosyl complexes have been widely studied in both homogeneous and heterogeneous systems with a view of finding the relationship among bonding, stability, and reactivity of the bound nitrosyl group.[1,2,5−7,11] The mode of coordination of the NO species is essentially controlled by the relative energies and the symmetry match between the π* and n orbitals of the NO ligand and orbitals of the d manifold of the TMI center.

The two limiting VB (valence bond) structures correspond to NO^+ and NO^- categories. Typically, a cationic nitrosyl ligand results in a nearly linear TMI−NO bond and a larger N−O stretching frequency (in comparison to the free NO molecule) while an anionic nitrosyl ligand is usually characterized by a bent end-on coordinated NO exhibiting a lower frequency of vibration. The bending of the nitrosyl ligand and the concomitant changes in electron density are of considerable importance in understanding the chemistry of nitrosyl compounds and the catalytic processes in which they are active. Generally, linear nitrosyls with ν_{NO} greater than ∼1850 cm^{-1} undergo nucleophilic attack on the nitrogen atom while bent nitrosyls undergo electrophilic attack.[5−7] The implications of the alternative coordination modes of NO coordinated to transition metals on its reactivity have been reviewed earlier.[5,6]

Despite its thermodynamic instability, nitric oxide is kinetically inert with respect to its decomposition into the elements, which requires a catalyst. Copper ions dispersed at the surface of metal oxides or within the framework of zeolites have shown a surprising activity for the direct catalytic decomposition and selective catalytic reduction (SCR) of NO.[4,8−10,12,13] It has been shown that copper-exchanged ZSM-5 zeolites catalyze both the thermal decomposition of NO into N_2 and O_2[8−10,12,13] and at room temperature its photocatalytic decomposition.[14,15] Most of the reported data suggest Cu^+ ions as catalytic centers.[2,4,10−15] Although the unique activity of exchanged Cu/ZSM-5 has been well established and reproduced, its origin is still a subject of debate, since many questions remain unanswered concerning the individual steps and the exact nature of the species involved.[4,8,9,16] Highly exchanged Cu/ZSM-5 catalysts are more active in NO decomposition,[17−19] but the coexistence of different oxidation and aggregation states of copper[18−22] makes it difficult to elucidate the structural properties related to the mechanism of this process. The mechanistic role of Cu species and CuNO intermediates can be best revealed if the system is well defined so that spectra of good quality can be obtained. This implies model studies on samples with low Cu content, since only in this case the status of the copper can be controlled.[11,20]

* To whom correspondence should be addressed.
† Present address: Faculty of Chemistry, Jagiellonian University, Cracow, Poland.
‡ Membre de l'Institut Universitaire de France.
⊗ Abstract published in *Advance ACS Abstracts,* May 1, 1997.

S1089-5647(97)00662-7 CCC: $14.00

TABLE 1: Experimental EPR Parameters of Cu^{2+}/ZSM-5 Centers and $Cu^{+}-NO$ Adducts

species	$g_\perp$	$g_\parallel$	$\lvert^{Cu}A_\perp\rvert$ (G)	$\lvert^{Cu}A_\parallel\rvert$ (G)	$\lvert^{N}A_\perp\rvert$ (G)	$\lvert^{N}A_\parallel\rvert$ (G)	ref
Cu^{2+}/ZSM-5	2.0614	2.305	22.3	165			this work
Cu^{2+}/ZSM-5	2.079	2.310	20.7	165			this work
$Cu^{+}-NO$/ZSM-5	1.999, 2.003, 1.889[a]		160, 155, 205[b] (149.5, 144.9, 181.8)[c]		30, 4.3, 5.5[d] (28, 4.0, 4.95)[c]		this work
$Cu^{+}-NO$/Y	2.034	1.99	177	238			37
$Cu^{+}-NO$/Y	2.009	1.89	190	240			29
$Cu^{+}-NO$/L	2.030	1.91	169	239			30
$Cu^{+}-NO/SiO_2$	2.030	1.94	112	166			38
$Cu^{+}-NO/SiO_2$	2.030	1.94	118	183			39
$Cu^{+}-NO/Tp^{RR'}$	1.99	1.83	62	107		27[e]	1

[a] g_x, g_y, and g_z, respectively. [b] $\lvert^{Cu}A_x\rvert$, $\lvert^{Cu}A_y\rvert$, and $\lvert^{Cu}A_z\rvert$, respectively. [c] These values are given in $10^{-4}cm^{-1}$. [d] $\lvert^{N}A_x\rvert$, $\lvert^{N}A_y\rvert$, and $\lvert^{N}A_z\rvert$, respectively. [e] $\lvert^{N}A_x\rvert$.

The spectroscopic characterization of the reactivity of NO with copper-exchanged ZSM-5 zeolite has already been reported.[2,11,23−25] The $Cu^{+}-NO$ bond is relatively weak and no substantial charge transfer between the metal ion and the ligand could be inferred from IR data. Furthermore, at room temperature the adduct is formed under low-pressure $p_{NO} < 3.75$ hPa (5 Torr). Upon increasing pressure, a second NO molecule coordinates to copper and a dinitrosyl species is formed.[2] M. Iwamoto and H. Hamada have shown that the decay of both mono- and dinitrosyl species correlates with the reaction rate of NO decomposition.[4,9] However, high-temperature IR studies of W. Hall and J. Valyon revealed that at 623−723 K, only mononitrosyl species can be detected.[24] Since the typical concentration of NO in exhaust gases is about 1000 ppm,[8,26] which corresponds to $p_{NO} < 1.33$ hPa (1 Torr), it is likely that for the real catalytic process the mononitrosyl adduct may become an important reaction intermediate.

The intrazeolitic $Cu^{+}-NO$/ZSM-5 complex is not the unique example of heterogeneous copper nitrosyl adducts, since similar species were also observed for Cu^{+}/Y and Cu^{+}/L zeolites.[27−30] The first stable homogeneous $Tp^{RR'}CuNO$ complexes ($Tp^{RR'}$ = tris(3-*R*,5-*R*′-pyrazolyl)hydroborate) was reported and spectroscopically characterized by C. Ruggiero et al.[1] Typically, the EPR spectra of the $Cu^{+}-NO$/Y and $Cu^{+}-NO$/L exhibit a distinctly lower resolution than $Cu^{+}-NO$/ZSM-5 with an unresolved ^{14}N hyperfine structure.

The aim of the present paper is to analyze relatively well-resolved EPR spectra of $Cu^{+}-NO$/ZSM-5, taking into account its low C_s symmetry. From the spin Hamiltonian parameters, the nature of the bonding and the electronic structure of the intrazeolitic $Cu^{+}-NO$ complex will be deduced. The relevance of this information for the mechanism of the catalytic NO decomposition will also be discussed. The present work is part of a more general study on the bonding and activation of small molecules to transition metal ions, which act as catalytically active sites on surfaces. In this respect, the surface coordination chemistry of NO is richer than that of many other simple molecules.

Experimental Section

The Cu/ZSM-5 samples (0.13 wt % Cu, Si/Al ratio = 23.3) were obtained by ion exchange with an aqueous copper nitrate solution as described in detail elsewhere.[2] The sample was then dehydrated at 673 K and reduced under 100 Torr of hydrogen at 603 K for 30 min and finally evacuated. A small amount of NO (about 1.33 hPa (1 Torr)) was adsorbed at 298 K, and next the sample was cooled to 77 K for recording of the EPR spectra. Prior to adsorption, NO was purified by the freeze−pump−thaw technique.

X band EPR spectra were recorded at 77 K on a Varian E-109 spectrometer with 100 kHz field modulation and equipped with a dual cavity. The g values were determined using a Varian pitch ($g = 2.0028$) as a reference standard. The analysis of Zeeman, hyperfine, and superhyperfine tensors was done by fitting computer-simulated line shapes to the experimental spectrum. Simulations were performed assuming initially coincident axes of **g** and hyperfine tensors with the SIM14A program[31] and then allowing for noncoincidence of axes with the POW program.[32] Both programs use second-order perturbation formula developed by S. Blinder[33] to calculate the energy levels while transition probabilities are treated to first order. A Lorentzian line shape and m^2 dependence of line widths was used to account for random distribution of the distances between CuNO paramagnets and **g** and **A** tensors dispersion[34] caused by microheterogeneity of the copper sites (vide infra). The simulation programs are complemented by minimization subroutines using a Nedler−Mead simplex method with no restrictions[35] and a grid search with adjustable steps.[36] A weighted least-squares error was used as a criterion for the best fit.

Results and Interpretation

EPR Spectra. Cu^{2+}-exchanged ZSM-5 zeolites dehydrated at 673 K exhibit a complex EPR spectrum owing to the presence of two distinct axial Cu^{2+} species with $g_\perp = 2.0614$, $g_\parallel = 2.305$, $A_\perp = 22.3$ G, $A_\parallel = 165$ G, and $g_\perp = 2.079$, $g_\parallel = 2.310$, $A_\perp = 20.7$ G, $A_\parallel = 165$ G (Table 1). These signals have been already reported and assigned[2] but with parameters not optimized by simulation.

After thermal reduction of the samples, a remarkable decrease in intensity of the spectrum is observed due to reduction of Cu^{2+} to Cu^{+} ions. However, some Cu^{2+} ions are still observed after reduction (Figure 1a). Additionally, at $g \approx 2$, a sharp signal due to carbonaceous radicals formed during reduction is also detected.[2] Upon contact of the sample with gaseous NO, a new intense spectrum appears (Figure 1b). Although it still exhibits weak features related to intact Cu^{2+}, which are clearly apparent in the low-field part of the spectrum (marked in Figure 1b by the asterisks), it is dominated by a new strong signal dramatically different from that of the parent Cu^{2+} ions. This signal consists of four strong lines with uneven spacings due to the overlap of "perpendicular" and "parallel" copper hyperfine features, suggesting that only one Cu ion is involved. In the high-field region, the outermost "parallel" $^{Cu}m_I = -3/2$ line is clearly observed. The overlapped lines corresponding to "perpendicular" $^{Cu}m_I = +1/2$ and "parallel" $^{Cu}m_I = +1/2$ and $+3/2$ transitions exhibit additional distinctly resolved splitting attributable to the coupling of the unpaired electron with the nitrogen nucleus.

Thus, the simultaneous presence of $^{63,65}Cu(I = 3/2)$ and ^{14}N-($I = 1$) hyperfine couplings clearly implies that the signal is due to a copper nitrosyl species formed upon interaction of Cu^{+} with NO. Moreover, despite the presence of two distinct copper sites in the parent sample, the presence of only one $Cu^{+}-NO$ species is detected. Two different Cu^{+} centers were also observed by IR to lead upon NO adsorption to one $Cu^{+}-NO$

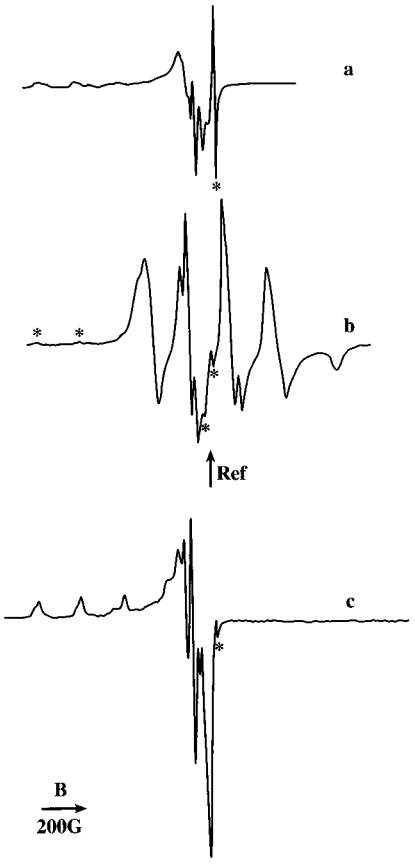

Figure 1. EPR spectra (X band) (a) of residual Cu^{2+} ions and carbon radicals present in the reduced Cu/ZSM-5 sample, (b) of the $Cu^{+}-NO$ adduct obtained after adsorption of 1.33 hPa (1 Torr) of NO on reduced Cu/ZSM-5 sample at 298 K, and (c) of Cu^{2+} ions reappearing upon subsequent oxidation by NO followed by evacuation at 473 K. The weak lines due to the superimposed impurity signals of Cu^{2+} (and carbon radical) are still visible, especially in the low-field part of the spectrum where they are unoverlapped. All spectra were registered at 77 K.

adduct.[11,20] Apparently, the broadening of the spectral lines prevents the detection of more than one species. This broadening is caused by the intrinsic heterogeneity of the copper sites in ZSM-5 as revealed by G. Spoto et al.[40] and in the case of EPR spectra by additional and unresolved superhyperfine interactions.[41] Therefore, even if more than one $Cu^{+}-NO$ adduct are formed, they have nearly the same structure, since neither EPR nor IR spectroscopies can distinguish them.

Other noteworthy features of the $Cu^{+}-NO$ spectrum are a distinct negative shift (with respect to the g_e value) of one of the **g** tensor components and unusually large values of the ^{63,65}-Cu splittings (Table 1). The latter are even greater than those initially observed for the Cu^{2+}, with the unpaired electron principally localized on the copper ion. These features completely rule out the assignment of this spectrum to a $Cu^{2+}-NO$ species.

The form of the experimental **g** tensor suggests that the $Cu^{+}-NO$ adduct may be, at first approximation, accounted for as a $^2\Pi$ state with the unpaired electron confined in the lower π^* antibonding orbital of the NO molecule.[28] Furthermore, the spectral parameters strongly suggest, as explained below, that the complex exhibits a bent end-on structure, which, though not always correctly recognized, may have important consequences for the reactivity of NO.

The paramagnetic $Cu^{+}-NO$ adduct is unstable and fades away with time, restoring after subsequent evacuation at 473 K the spectrum characteristic for the Cu^{2+} centers (Figure 1c) with a $d_{x^2-y^2}$ ground state. This indicates that an intramolecular electron-transfer process is associated with the reductive transformation of the NO ligand.

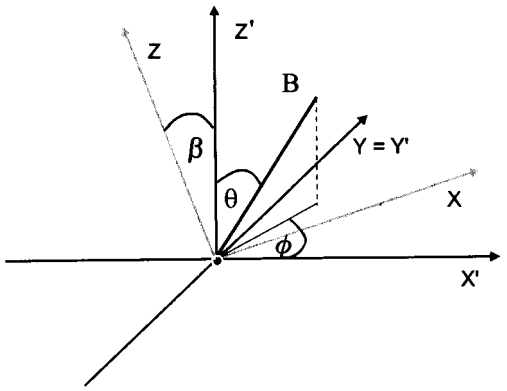

Figure 2. Reference axis system for $Cu^{+}-NO$ adducts used for simulation and interpretation of the spin Hamiltonian parameters. The (x', y', z') axes refer to the **g** tensor, while (x, y, z) axes refer to the Cu shf tensor. Both systems are noncoincident in xz plane, and the integration was carried out in the north−south octant.[23]

Determination of the Spin Hamiltonian Parameters. The low C_s local symmetry of the $Cu^{+}-NO$ adduct implies a noncoincidence of those principal axes of the **g** and ^{Cu}**A** tensors that are lying in the symmetry plane, while the axis normal to the mirror plane is necessarily common to both tensors. Therefore, for the analysis of the spin Hamiltonian parameters of the intrazeolitic $Cu^{+}-NO$ complex to be rigorous, a monoclinic system of the principal axes for the **g** and ^{Cu}**A** tensors is appropriate.[42]

In our stepwise analysis of the problem, the symmetry was initially approximated as orthorhombic, and the preliminary Cu superhyperfine structure (shfs) constants were first estimated via simulation without correction for the different orientations of the axis systems. This means that the Cu shfs was determined within the **g** tensor principal axes.[42,43] As a result, only that component of the ^{Cu}**A** value that corresponds to the axis perpendicular to the mirror plane can be obtained directly, while the other two related to in-plane axes are over- and underestimated by an extent dictated by the value of the rotation angle β (see below). Although the gross features of the EPR spectrum of the adduct were reproduced using this approach, the quality of the best fit was still found to be unsatisfactory (crude reproduction of the line intensities), implying that the invoked tensors are really not coaxial,[42] as suggested by symmetry considerations.

The simulation of the EPR spectrum of the $Cu^{+}-NO$ species was next refined on the basis of the following spin Hamiltonian,

$$\hat{H} = \beta_e B\mathbf{g}S + \sum_{i=Cu,N} S^i \mathbf{A}^i I \qquad (1)$$

using the axes system described in Figure 2, where the **g** and ^{Cu}**A** tensors share the y axis, but with x and z axes differing by the Euler angle β. The best fit parameters are reported and assigned in Table 1. A satisfactory match with the experimental line positions and intensities was achieved for $\beta = 40°$ (Figure 3). The features marked by asterisks come from a superimposed signal due to residual Cu^{2+} (see the low-field part of the spectrum in Figure 1b) that could not be taken into account in the simulation by our program. The contribution of the Cu^{2+} species to this spectrum is better revealed in the EPR spectra with higher (1.9 wt %) copper loading,[2] where pronounced lines of the Cu^{2+} ions are easily detected, allowing us to assign the spin Hamiltonian parameters.

The anisotropies of both Cu shfs and **g** tensors are distinctly pronounced. The **g** tensor values are similar to those measured

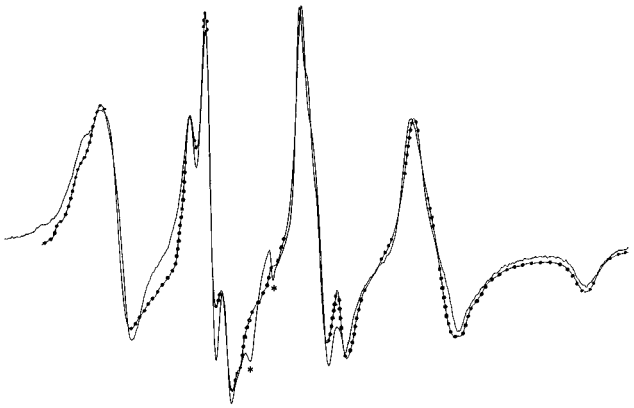

Figure 3. Computer simulation (line with black points) of the $Cu^{+}-NO$ EPR spectrum (solid line). Features marked by an asterisk correspond to residual minor Cu^{2+} and carbon radical lines that were not taken into account during simulation.

for NO adsorbed on a variety of metal oxides such as Al_2O_3 and $SiO_2-Al_2O_3$,[44] TiO_2,[45] and ZnO[46] and Na/Y[28,29] and Cu/L zeolites[30] (Table 1). In all those cases, two of the **g** components are around the free electron g value ($g_e = 2.0023$) while the third one (whose direction is along the internuclear N−O axis) is definitely lower, between 1.83 and 1.94.

Discussion

Symmetry Considerations. To interpret the EPR data, we have developed a molecular orbital scheme for the $Cu^{+}-NO$ adduct inspired by the earlier extended Hückel calculations of R. Hoffmann et al.[3]

The exchangeable cation sites in ZSM-5 are not as well-known as in other zeolites,[47] and the exact localization of Cu^{2+} ions in dehydrated ZSM-5 zeolites is a subject of many investigations by EPR, ESEM, UV−vis, EXAFS, IR, and XPS methods.[47−53] It is now generally accepted that for fully dehydrated zeolites at low copper loading Cu^{2+} ($3d^9$) species are localized in the center of the rings with square pyramid and square planar coordinations. These coordinations lead to crystal field stabilization energy (CFSE) and Coulombic interactions with two Al-substituted T sites of the zeolitic ring.[47,48,50−52] Schoonheydt suggests that the square pyramid arrangement is close to that of the E sites of C_{4v} symmetry identified earlier in mordenites.[47] Following these assignments, we also attribute the C_{4v} arrangement to Cu^{2+} ions in ZSM-5 zeolites. The localization of the monovalent Cu^{+} ($3d^{10}$) species formed by reduction of Cu^{2+} is likely to be different.[11,20,54] Since they are not stabilized by the crystal field and interact with only one $[AlO_4]^{-}$, the Cu^{+} move toward the side of the rings where the negative charge $Si-O^{-}-Al$ centers possessing a C_s symmetry and low coordination number (CN = 2 or 3) are located.[11,20,54,56] Such a location for the cuprous ions was experimentally established by A. Zecchina and co-workers using jointly several techniques.[11,20] Furthermore, these assignments of Cu^{2+} and Cu^{+} species as well as the migration of Cu^{+} toward $Si-O^{-}-Al$ sites are well accounted for by theoretical calculations.[55,56] Thus, the adsorption of NO on Cu^{+} leading to a bent mononitrosyl species will not change the local C_s site symmetry.

Crystallographic and chemical studies have established that a number of coordination geometries exist for the NO ligand bound to various transition metal ions[3,6,57] the predominant being the bent and linear structures. From the analysis of the experimental EPR data (vide infra) and also by analogy with the X-ray crystal structure of the homogeneous Tp $^{RR'}$CuNO complexes,[1] the linear geometry can be ruled out, leaving the bent end-on nitrosyl as the most likely species. From the two possible cases for the Cu−N−O angle ($\pi - \alpha$) and ($\pi/2 + \alpha$),

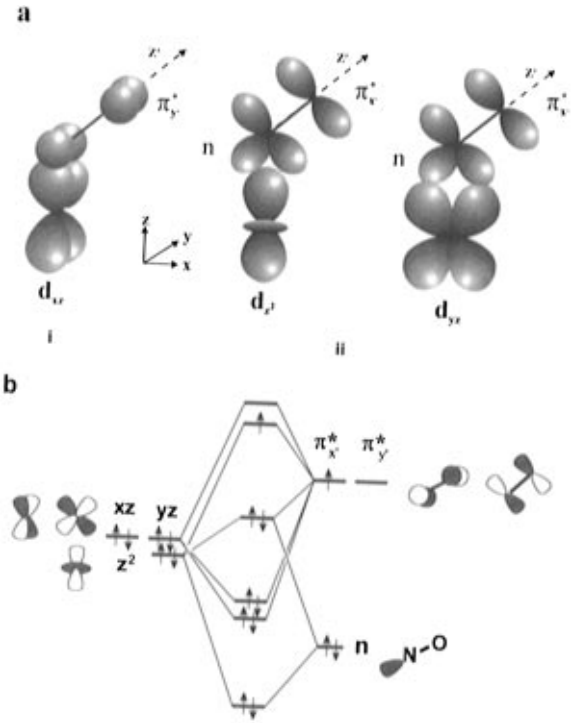

Figure 4. (a) Overlap of the Cu and NO orbitals involved in the formation of SOMO (Φ_a) and LUMO (Φ_{as}): (i) the interaction of the $3d_{yz}$ with $\pi_{y'}$*(2p) orbitals producing Φ_{as}; (ii) the overlap of the $3d_{z^2}$ and $3d_{xz}$ with $\pi_{x'}$*(2p) and lone pair n orbitals giving the Φ_a MO. (b) Proposed molecular orbital diagram for the $Cu^{+}-NO$ adduct.

the latter can be rejected on the basis of arguments developed in the discussion (vide infra) and on the basis of the earlier work of C. Chao and J. Lunsford[29] and J. Enemark and R. Feltham.[57]

According to R. Hoffmann et al.,[3] the apical nitrosyl group is reduced to its essentials: a donor lone pair n on nitrogen and a pair of higher lying acceptor 2p π* orbitals. Considering that the $Cu^{+}-NO$ complex belongs to the C_s point group, an overlap of the lone pair n with the Cu d_{z^2} orbital produces a four-electron closed-shell destabilizing interaction (Figure 4a) that is decreased upon bending the Cu−N−O species by moving NO in the xz plane. At the same time, a new interaction between d_{z^2} and $\pi^*_{x'}$ absent in the linear geometry develops. The symmetric $\pi^*_{x'}$ and antisymmetric $\pi^*_{y'}$ orbitals display a π-type overlap with the d_{xz} and d_{yz} orbitals of copper, respectively. The d_{xz},$d_{yz}-\pi^*_{x',y'}$ interactions are stabilizing and will be maximized in the linear geometry (Figure 4). The determining factor in the bending lies in the energies of the metal orbitals d_{z^2} d_{yz}, and d_{xz} relative to the energies of the nitrosyl n and π* orbitals. The proposed molecular orbital diagram for the $Cu^{+}-NO$ adduct is shown in Figure 4b. The $d_{x^2-y^2}$ orbital is located below the SOMO in order to conform with the EPR data, which indicate that an unpaired electron is mainly located on NO (see analysis of the ^{Cu}**A** and ^{14}**N** superhyperfine and hyperfine tensors, respectively).

From the orbitals that are responsible for the NO linkage, the following two predominantly account for the observed **g** tensor and the hyperfine structure:

$$\Phi_s = c_1|z^2\rangle + c_2|xz\rangle + c_3|4s\rangle + b_1|\pi^*_{x'}\rangle + b_2|n\rangle$$

$$\Phi_{as} = c'_1|yz\rangle + b'_1|\pi^*_{y'}\rangle \qquad (2)$$

where the coefficients, neglecting overlap (to make the problem tractable), are normalized to 1. Since the d_{z^2}, 4s, and d_{xz} orbitals have the same A′ symmetry species in the point group C_s, they all contribute to Φ_s.

^{Cu}A Superhyperfine Tensor. The Cu shfs tensor can be expressed in terms of three different contributions

$$^{Cu}\mathbf{A} = a_{iso} + \mathbf{A}_{dip} + \mathbf{T} \quad (3)$$

where a_{iso} represents the Fermi contact term, **T** the anisotropic part of the copper shf interaction, and $\mathbf{A}_{dip}$ the dipolar tensor[58] approximated as

$$A_{dip(x,y)} = -g_e\beta_e g_{Cu}\beta_N/r^3$$

$$A_{dip(z)} = 2g_e\beta_e g_{Cu}\beta_N/r^3 \quad (4)$$

The principal values of this tensor have been estimated (see below) using the distance r of the Cu−NO bond length equal to ∼1.8 Å.[1]

A further analysis of the shfs tensor requires a knowledge of the sign of the Cu coupling constants. The only reasonable alternative of Cu shfs is that the three components must have the same sign (either positive or negative), since all other combinations lead to unacceptable results with the unpaired electron mainly on copper while there is a good evidence from the **g** tensor that it is largely delocalized onto the NO moiety.

The assumption that the SOMO is the antisymmetric Φ_{as} orbital implies that the d_{yz} orbital is involved and that the maximal value of the shfs being negative corresponds to the x axis ($T(d_{yz}) \propto Pc_1^2|-4/7\ (x),\ +2/7\ (y),\ +2/7\ (z)|$). The value of a_{iso} is then expected to be negative and small, since 4s(a′) does not mix with d_{yz}(a″). The observed deviations from axial symmetry of the Cu shfs tensor may then arise from polarization of the σ-bonding Φ_s by the unpaired electron localized on Φ_{as}.[59]

If the SOMO is assumed to be a symmetric Φ_s orbital, then the Cu shfs is expected to be positive owing to the delocalization of the unpaired electron density onto d_{z^2} and 4s orbitals, which should in turn produce a positive a_{iso} value large enough to compensate for a possible negative contribution arising from polarization (vide infra). This choice of the SOMO implies a $\pi-\alpha$ geometry of the Cu^+-NO adduct in order to be consistent with the experimental evidence that the maximal Cu coupling is connected with the direction (z' axis) of maximal shift of the g value. According to this model, the largest ^{14}N coupling is expected to be along the x' direction, again consistent with experimental observation. Thus, according to eq 3, we can decompose the experimental Cu shfs tensor in the following way:

$$\begin{vmatrix} +149.5 \\ +144.9 \\ +181.8 \end{vmatrix} = +158.5 + \begin{vmatrix} -0.8 \\ -0.8 \\ +1.6 \end{vmatrix} + \begin{vmatrix} -8.2 \\ -12.8 \\ +21 \end{vmatrix}$$

where all the values are given in $cm^{-1} \times 10^{-4}$ (Table 1).

The signs of the principal values of the shfs (^{Cu}**A** tensor) were taken to be positive in order to conform with the positive value of a_{iso} that is due largely to direct delocalization of the unpaired electron density onto the 4s orbital and the orientation of the anisotropic Cu tensor.

Isotropic Cu Superhyperfine Tensor. In principle, the isotropic copper coupling (a_{iso}) arises from polarization of the filled inner s orbitals, giving negative contributions to a_{iso}, and from the admixture of 4s character in the molecular orbital containing the unpaired electron (SOMO), giving a positive contribution to the superhyperfine coupling. The actually observed value of $a_{iso} = 172.8$ G (158.5×10^{-4} cm^{-1}) is thus a balance of all these contributions. Even a small component of 4s in the SOMO would produce, however, a quite substantial contribution to the isotropic Cu shfs because of the large value of the copper Fermi contact ($^{Cu}A°_{4s} = 1767$ G [58]). An obvious disparity exists in the comparison of the experimental value of a_{iso} of Cu^+-NO with the corresponding value found for the parent Cu^{2+} centers. The core polarization of the filled s orbitals is typically assumed to be the major source for the isotropic hyperfine value for the Cu^{2+}/ZSM-5 tetragonal species with a $d_{x^2-y^2}$ ground state,[60] and $a_{iso} = 70$ G is obtained for the parent Cu^{2+}. This value is ca. 2.5 times smaller than that observed for the Cu^+-NO adduct (172.8 G) despite the fact that in this case the unpaired electron is almost entirely localized on Cu^{2+}. Thus, if only the spin polarization mechanism were operating in Cu^+-NO, then the expected value of a_{iso} would be on the order of 8 G, a value much lower than what is actually observed. These results indicate the involvement of the 4s orbital in the SOMO, confirming simultaneously the A′ symmetry of the semioccupied orbital.

Although both components of the resultant isotropic Cu coupling, i.e., the core polarization and the admixture of 4s, tend to cancel each other, making the measured a_{iso} of copper less reliable, their individual contributions can be still assessed from the following equation:[61]

$$a_{iso} = P(\kappa_s\rho^{4s} - \kappa_d\rho^{3d}) \quad (5)$$

where $P\kappa_s = 0.200$ cm^{-1} [62] represents the contribution of the copper 4s spin density and $P\kappa_d = 0.0150$ cm^{-1} accounts for polarization of inner-shell s orbitals by spin density in copper 3d orbitals. This latter value was estimated from the isotropic copper coupling of the parent Cu^{2+} signal, using the following set of equations:[63]

$$\rho^{3d} = (7/6)[-(A_{||} - A_\perp)/P + (g_{||} - 2.0023) - 5(g_\perp - 2.0023)/14] \quad (6a)$$

$$\kappa_d = (1/\rho^{3d})[-A_{||}/P - 4/7\rho^{3d} + (g_{||} - 2.0023) + 3(g_\perp - 2.0023)/7] \quad (6b)$$

and $P = 0.036$ cm^{-1}. For the Cu^+-NO adduct, as shown in the next section, $\rho^{3d} = 0.1$. Substitution of the numerical values for $P\kappa_s$, $P\kappa_d$, and ρ^{3d} into eq 5 leads to $\rho^{4s} = c_3^2 \approx 0.1$. This allows a satisfactory estimate of the 4s contribution to the covalency of the Cu^+-NO Φ_s orbital (SOMO).

Anisotropic Cu Superhyperfine Tensor. The Cu anisotropic shfs tensor **T** is distinctly nonaxial and the compatible choice of signs and axes in our assignment leads to T_{zz} being positive. This restricts the copper 3d contributions to combinations of d_{z^2} and d_{xz} atomic orbitals.

When the contribution of the copper atomic orbitals to the orbital containing the unpaired electron is described by eq 2 (the wave function Φ_s), the anisotropic Cu tensor components are given by

$$T_{ij} = \frac{2}{7}P\rho^{3d}l_{ij} \quad (7)$$

where P has the usual meaning $P = g\beta g_{Cu}\beta_N 1/\langle r^3\rangle$ and the l_{ij} components have the following form[61]

$$l_{xx} = -c_1^2 + c_2^2$$

$$l_{yy} = -c_1^2 - 2c_2^2$$

$$l_{zz} = 2c_1^2 + c_2^2$$

$$l_{xz} = l_{zx} = \sqrt{3}c_1c_2 \quad (8)$$

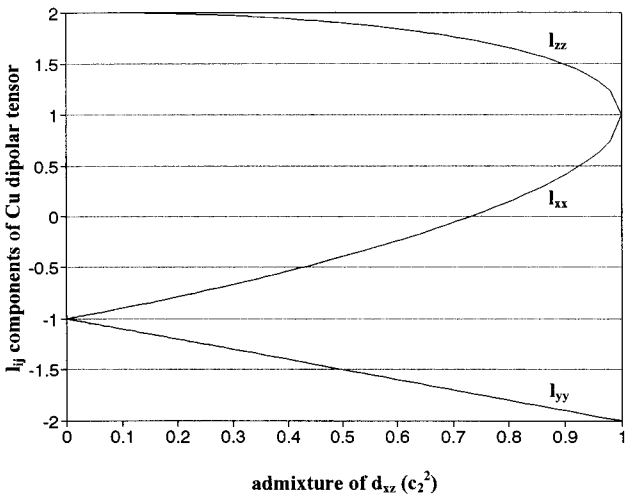

Figure 5. Values of the dipolar hyperfine tensor components l_{ij} as a function of c_2^2, c_2 being the admixture coefficient of d_{xz} orbital.

The **T** tensor may be diagonalized by rotation about the common axis y by the angle β_A, given by

$$\tan 2\beta_A = -2c_2/(3c_1) \tag{9}$$

to provide the principal values

$$T_{yy} = \frac{2}{7}P\rho^{3d}(-c_1^2 - 2c_2^2)$$

$$T_{xx} = \frac{2}{7}P\rho^{3d}(-c_1^2 + c_2^2)\cos^2\beta_A + (2c_1^2 + c_2^2)\sin^2\beta_A + 2\sqrt{3}c_1c_2\sin\beta_A\cos\beta_A$$

$$T_{zz} = \frac{2}{7}P\rho^{3d}(-c_1^2 + c_2^2)\sin^2\beta_A + (2c_1^2 + c_2^2)\cos^2\beta_A - 2\sqrt{3}c_1c_2\sin\beta_A\cos\beta_A \tag{10}$$

which are plotted in Figure 5 as a function of the admixture of d_{xz} orbital. Separation of the d_{z^2} and d_{xz} contributions to the copper shfs may be next performed by finding such a combination of those orbitals for which theoretical ratios of the l_{ij} components reproduce the experimental values. The best fit was found to occur for the 0.21/0.79 ratio of the d_{xz} (c_2^2) and d_{z^2} (c_1^2) orbitals, respectively.

Comparison of the experimental and calculated (eq 10) anisotropic superhyperfine tensors gives $P\rho^{3d} = 36.73 \times 10^{-4}$ cm^{-1}, which, taking $P = 360 \times 10^{-4}$ cm^{-1},[63] leads to $\rho^{3d} = 0.102$. Thus, the total copper 3d character of the SOMO is equal to 0.2 (0.1 on 4s, 0.021 on d_{xz}, and 0.079 on d_{z^2}). The contribution of the 4p orbital to the anisotropic shfs tensor has been ignored, since $\langle r^{-3}\rangle_{4p}$ is considerably smaller than $\langle r^{-3}\rangle_{3d}$. This omission seems to be justified on the basis of earlier work.[61]

Taking the angle β as the sum of the absolute magnitude of β_g and β_A,[64] the angles $\beta = 40°$ (found via simulation) and $\beta_A = 22°$ (computed using eq 9) can be then used to obtain the bending angle α of the Cu$^+$−NO moiety. Because the $g_{z'}$ axis is directed along the NO bond, the **g** tensor z' axis is displayed from the corresponding molecular z axis (Figure 4a) by the angle α. Therefore, $\beta = |\alpha| + |\beta_A|$ yields $\alpha = 18°$, a value close to that determined from X-ray data (16.5°) for the Tp$^{RR'}$CuNO complexes.[1]

^{14}N Hyperfine Tensor. Further information concerning the nature of the NO bonding to Cu$^+$ is obtained from the analysis of the ^{14}N hfs. The largest value of the nitrogen hyperfine tensor corresponds to the direction determined by the 2π orbital occupied by the unpaired electron (x' direction). The sign and magnitude of a_{iso} are a function of the spin density on both N and O atoms, and by analogy with the isoelectronic N_2^- radical, the sign is assumed to be positive.[65] As usual, the nitrogen hyperfine tensor may be decomposed into two parts: anisotropic and isotropic. The three components of the hyperfine interaction have the same sign as previously reported for nitrosyl CpM(CO)$_2$NO$^-$ (M = Cr, Mo) complexes having very similar ^{14}N hfs tensors.[66] This choice gave the only physically reasonable combination, which is consistent with the positive value of a_{iso}, the dominant spin density delocalization on the NO and also, with the antibonding nature, between N and O, of the orbital containing the unpaired electron.

TABLE 2. Spin Density Distributions ρ_i (i = Cu, N, O) in the Cu$^+$−NO Adduct

orbital	ρ_{Cu}	ρ_N	ρ_O
s	∼0.1	∼0.02	
π^*(2p)		0.51	0.25[a]
p_z		0.02	
d_{xz}	0.021		
d_{z^2}	0.079		

[a] This value is derived assumming the total spin density of N, Cu, and O atoms is unity.

We can decompose the observed ^{N}**A** hfs tensor to get the traceless anisotropic components along the x' and z' directions.

$$\begin{vmatrix}+28\\+4.0\\+4.95\end{vmatrix} = +12.3 + \begin{vmatrix}+15.7\\-8.3\\-7.4\end{vmatrix} = 12.3 + \begin{vmatrix}+16\\-8\\-8\end{vmatrix} + \begin{vmatrix}-0.31\\-0.31\\+0.63\end{vmatrix}$$

where all the values are given in cm^{-1} × 10^{-4} (Table 1).

The resultant spin density on nitrogen 2p orbitals is equal to $\rho^{2p} = (2b_N + 2a_N)/B_N^\circ = (17.1\text{ G} + 0.71\text{ G})/33.5\text{ G} = 0.53$, where $2b_N = 16 \times 10^{-4}$ cm^{-1} (171.1 G) and $2a_N = 0.63 \times 10^{-4}$ cm^{-1} (0.71 G) are the principal components of the experimental anisotropic ^{14}N hfs tensors along the x' and z' directions, while $B_N^\circ = 33.5$ G refers to the corresponding atomic value.[67] The analysis of the traceless tensors along x' and z' indicates that the unpaired electron is mainly confined to the nitrogen $2p_{x'}(\pi^*)$ orbital ($b_1^2 = 17.1\text{ G}/33.5\text{ G} = 0.51$), but participation of the $2p_{z'}$ orbital is not negligible ($b_2^2 = 0.71\text{ G}/33.5\text{ G} = 0.02$).

As usual, the isotropic nitrogen coupling is more difficult to interpret, since it arises both from direct contribution of the nitrogen 2s orbital to the SOMO and from polarization of filled s orbitals. To transform the spin density on the π^*(2p) orbital of N into isotropic hyperfine coupling constants, a two-term equation advanced by T. Hunter and M. Symons[68] has been used:

$$\frac{100^N a_{iso}}{^N A_{iso}^0} = \rho_N U^N + (1 - \rho_N - \rho_{Cu})U_{NO}^0 \tag{11}$$

where ρ_N is the spin density on the nitrogen 2p orbital and U^N and U_{NO}^0 are polarization and adjacent-atom polarization constants, respectively. In this formula, the residual unpaired electron density on the oxygen atom of NO has been estimated by summing the spin densities on N, O, and Cu atoms to unity. For NO, the magnitude of the U_N and U_{NO}^0 constants are 2.2 and −2.0, respectively.[67,68] As a result, the spin densities on nitrogen $\pi^*(2p) = 0.51$ and on oxygen $\pi^*(2p) = 0.25$ produce an isotropic splitting equal to 3.4 G, leaving, in order to be consistent with the experimental a_{iso} value, about 9 G for the direct delocalization contribution. The latter value leads to a 2s spin density equal to $^9/_{557} \approx 0.02$, which is comparable to that found on the $2p_{z'}$ orbital of the NO lone pair. (The spin density distributions in the Cu$^+$−NO adduct are summarized in Table 2.) This means that the NO contribution to the SOMO

consists of a combination of the dominant $2\pi^*$ and the minor lone pair n orbitals and that the hybridization is appreciable.

It is worth noting that the bending angle α calculated from the sp^n hybridization ratio ($\alpha = \pi - 2\cos^{-1}(n^2 + 2)^{-1/2} = 160°$ [65]) is equal to 20°, in good agreement with the value $\alpha = 18°$ derived from the analysis of the copper shfs. Since for the observed hybridization ratio, this equation gives only approximate results, we think that such a good agreement may be in part fortuitous. A similar analysis based on the nitrogen hfs has been carried out on other transition nitrosyl compounds, revealing the presence of a bent M−NO geometry.[7]

g Tensor. The **g** tensor data are in accordance with the results of the hfs and shfs analyses. The comparison of the **g** principal values of Cu^{2+}/ZSM-5 and Cu^+-NO/ZSM-5 indicates that the **g** tensor of the adduct is governed by the presence of an unpaired electron on the NO, which corroborates the conclusions already derived earlier from shfs and hfs analysis. There is a significant unquenched orbital angular momentum about the NO internuclear axis z' ($\Delta g_{z'} = -0.113$). Such a large negative g shift observed along this direction is due to the spin−orbit interaction between the SOMO and a low-lying LUMO (another pair of the π^*) of the Cu^+-NO complex. (However, the close lying $d_{x^2-y^2}$ orbital does not contribute to $\Delta g_{z'}$, since it is not coupled by L_z with SOMO). This provides a clear evidence for the tilt geometry of the Cu^+-NO species. Indeed, the lowering of symmetry upon bending lifts the degeneracy of the NO π^* levels by the amount Δ. The splitting of both π^* energy levels is manifested by the **g** tensor shifts in the EPR spectrum according to the theoretical expressions,[45] valid strictly for the case of electrostatic interaction with the adsorption center:

$$g_z = g_e - 2\left[\frac{\lambda^2}{\lambda^2 + \Delta^2}\right]^{1/2}$$

$$g_{x,y} = g_e\left[\frac{\Delta^2}{\lambda^2 + \Delta^2}\right]^{1/2} \qquad (12)$$

where λ is the spin−orbit coupling constant of nitrogen, g_e the free electron value, and Δ the splitting of the two 2p π^* orbitals which have been defined in Figure 4b. Owing to the delocalization of the unpaired electron onto the Cu ion, this equation should be adjusted in order to account for bond covalency. Therefore, for calculating the Δ parameter, a modified expression

$$g_z = g_e - 2b^2\left[\frac{\lambda^2}{\lambda^2 + \Delta^2}\right]^{1/2}$$

was used, which is analogous to that previously applied to analyze the **g** tensor of cobalt superoxo adducts.[59] From the experimentally observed $\Delta g_{z'}$ shift and the values 0.015 eV for λ [46] and 0.8 for the covalency factor b^2 (determined from the shfs) the splitting Δ was found to be 0.24 eV. This value, close to $\Delta = 0.21$ eV observed for NO adsorbed on a dehydrated Na/Y zeolite, is substantially smaller from that found for NO on decationated Y zeolites ($\Delta = 0.6$ eV) or on dehydrated γ-alumina ($\Delta = 0.75$ eV).[44,46] In the latter case, NO is believed to be adsorbed on trivalent Al centers. The low value of $\Delta = 0.24$ eV is characteristic of the surface crystal field produced by a monovalent center, providing additional support for Cu^+-NO formulation of the copper nitrosyl adduct.

Possible Implications of the Coordination Mode on Catalysis. Under typically low p_{NO} pressures and real NO decomposition conditions, which favor the copper mononitrosyl species, the N−N bond formation might be accomplished only if the Cu^+-NO adduct can act as the site of formation of appropriate intermediates (e.g., hyponitrate) containing two adjacent nitrogens.

The electronic structure of the mononitrosyl Cu^+-NO can strongly influence its reactivity. Thus, a low gap between the SOMO and either the LUMO or the $d_{x^2-y^2}$ orbital (Figure 4b) indicates an unstable species, as experimentally observed (see EPR Spectra section in Results and Interpretation). As discussed earlier, this gap and concomitant changes in electron density distribution on the NO moiety are quite sensitive to the bending of the Cu^+-NO species. The bending lowers the symmetry of the Cu^+-NO adduct, allowing the mixing of π and σ orbitals (partial sp^n hybridization), which removes certain restrictions imposed by orbital symmetry conservation rules.[69] This type of coordination is characterized by a low frequency of bending oscillation, which typically is situated within the 400−700 cm^{-1} region,[70] so the corresponding vibrational levels may be accessible even at moderate temperatures.

Upon coordination of NO to Cu^+, a redistribution of the electron density occurs. The resulting mismatch of the new electronic structure to the former nuclear configuration leads in turn to the change of the activation energy of processes involving nuclear displacements (e.g., loosening of the N−O bond).[71,72] As a result, the relaxed NO molecule acquires some largely localized negative charge and becomes more prone to further chemical transformations.[71] These modifications open a new possibility of the reaction pathway involving an electrophilic attack of adsorbed NO by gas-phase NO (outer-sphere mechanism). The largest electron density in the SOMO on nitrogen (0.55) implies that this atom constitutes a preferential site for such an attack. It is likely that the vibrational preactivation of the Cu^+-NO species, by excitation into higher bending states and the accompanying flow of the electron density from the metal to the NO ligand, which transiently increase the negative charge on the nitrogen atom, will facilitate this reaction. The copper nitrosyl adduct becomes thereby more amenable for the electrophilic attack by NO initiating the formation of a N−N bond (Scheme 1).[6,7] At a certain point, this process becomes equivalent to the intramolecular reduction of NO by monovalent copper and the formation of the transient $Cu^{2+}N_2O_2^-$.

SCHEME 1

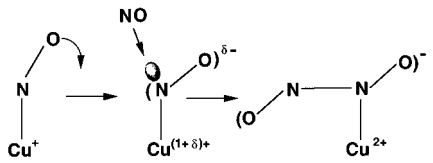

During this sequence, by analogy with the electrophilic oxidation of nitrosyl complexes by gas-phase NO,[7] it is assumed that the Cu−N bond is not broken and that the free NO molecule attacks the bent nitrosyl via its nitrogen atom. As a result, an intermediate hyponitrite $^-(ON-NO)$ is formed, which is expected to be in a *trans* configuration.[73] In the presence of NO, the hyponitrite readily decomposes into N_2O and NO_2^- as revealed earlier by IR.[2,11] As a result, the surface copper complex becomes again paramagnetic with the $d_{x^2-y^2}$ orbital being the new SOMO, which explains the reappearance of the Cu^{2+} EPR signal in Figure 1c.

This outer-sphere mechanism is, to a large extent, compatible with that advanced earlier for copper dinitrosyl intermediates,[11] but it suggests an alternative pathway along which the N−N bond may be formed under low pressures of NO on isolated copper centers. The bent structure of the Cu^+-NO adduct also accounts for how the extra electron density present on the nitrogen is functional in the formation of this bond.

Conclusions

The interaction of NO with copper-exchanged ZSM-5 zeolite gives rise to a paramagnetic Cu^+-NO adduct with a characteristic EPR spectrum with well-resolved[63,65] Cu and ^{14}N hyperfine structures. The analysis of copper and nitrogen shfs and hfs couplings respectively enables us to develop a semiquantitative molecular orbital correlation model and to predict the structure of the adduct. It is shown that Cu^+-NO is a bent η^1 complex in which copper remains monovalent and nitric oxide carries most of the unpaired spin density. From the analysis of the coupling constants, the detailed structure of the SOMO, including spin distribution, has been obtained, providing insight into the nature of the Cu^+-NO bonding and of its geometric structure. It is proposed that this particular bent η^1 structure at low p_{NO} values appears functional in the formation of a N−N bond via an electrophilic attack by gas-phase NO at the nitrogen atom of Cu^+-NO and opens an outer-sphere pathway for NO decomposition.

Acknowledgment. Z.S. is grateful to the Ministère de l'Enseignement Supérieur et de la Recherche and the Université P. et M. Curie for an invited professorship (PAST program).

References and Notes

(1) Ruggiero, C. E.; Carrier, S. M.; Antholine, W. E.; Whittaker, J. W.; Cramer, C. J.; Tolman, W. B. *J. Am . Chem. Soc.* **1993**, *115*, 11285.
(2) Giamello, E.; Murphy, D.; Magnacca, G.; Morterra, C.; Shioya, Y.; Nomura, T.; Anpo, M. *J. Catal.* **1992,** *136*, 510.
(3) Hoffmann, R.; Chen, M. M. L.; Elian, M.; Rossi, A. R.; Mingos, P. M. *Inorg. Chem.* **1974**, *13*, 2666.
(4) Iwamoto, M.; Hamada, H. *Catal. Today* **1991**, *10*, 57.
(5) Eisenberg, R.; Meyer, C. D. *Acc. Chem. Res.* **1975**, *8*, 27.
(6) Eisenberg, R.; Hendriksen D. E. *Adv. Catal.* **1979**, *28*, 79.
(7) Michael, D.; Mingos, P.; Sherman, D. J. *Adv. Inorg. Chem.* **1989**, *34*, 293.
(8) Shelef, M. *Chem. Rev. (Washington, D.C.)* **1995**, *95*, 209.
(9) Iwamoto, M.; Hamada, H. *Stud. Surf. Sci. Catal.* **1990**, *54*, 121.
(10) Li, Y.; Hall, W. K. *J. Phys. Chem.* **1990,** *94*, 6145.
(11) Spoto, G.; Zecchina, A.; Bordiga, S.; Ricchiardi, G.; Martra, G. *Appl. Catal. B* **1994**, *3*, 151.
(12) Iwamoto, M.; Yahiro, H.; Mine, Y.; Kagawa, S. *Chem. Lett*. **1989**, 213.
(13) Witzel, F.; Still, G. A.; Hall, W. K. *Stud. Surf. Sci. Catal.* **1994**, *84C*, 1513.
(14) Anpo, M.; Nomura, T.; Shioya, Y.; Giamello, E.; Murphy, D.; Che, M. *Proc. Int. Congr. Catal*, *10th* **1993**, 2155.
(15) Anpo, M.; Matsuoka, M.; Shioya, Y.; Yamashita, H.; Giamello, E.; Morterra, C.; Che, M.; Patterson, H. H.; Webber, S.; Ouellette, S.; Fox, M. A. *J. Phys. Chem.* **1994,** *98*, 5744.
(16) Valyon, J.; Hall, W. K. *J. Catal.* **1993**, *143*, 520.
(17) Kharas, K. C. C.; Liu, D.-J.; Robota, H. J. *Catal. Today* **1995**, *26*, 129.
(18) Iwamoto, M.; Yahiro, H.; Tanada, K.; Mizumo, N.; Mine, Y.; Kagawa, S. *J. Phys. Chem.* **1991,** *95*, 3727.
(19) Li, Y.; Hall, W. K. *J. Catal.* **1991**, *129*, 202.
(20) Lamberti, C.; Bordiga, S.; Salvalaggio, M.; Spoto, G.; Zecchina, A.; Geobaldo, F.; Vlaic, G.; Bellatreccia, M. *J. Phys. Chem. B* **1997**, *101*, 344.
(21) Kuroda, Y.; Yoshikawa, Y.; Konno, S.; Hamano, H.; Maeda, H.; Kumashiro, R.; Nagao, M. *J. Phys. Chem.* **1995,** *99*, 10621.
(22) Iwamoto, M.; Yahiro, H.; Mizuno, N.; Zhang, W.-X.; Mine, Y.; Furukawa, H.; Kagawa, S. *J. Phys. Chem.* **1992,** *96*, 9360.
(23) Cheung, T.; Bhargava, S. K.; Hobday, M.; Foger, K. *J. Catal.* **1996**, *158*, 301.
(24) Hall, W. K.; Valyon, J. *Catal. Lett.* **1992**, *15*, 311.
(25) Valyon, J.; Hall, W. K. *J. Phys. Chem.* **1993,** *97*, 1204.
(26) Taylor, K. C. *Catal. Rev. Sci. Eng.* **1993**, *35*, 61.
(27) Lunsford, J. H. In *The Catalytic Chemistry of Nitrogen Oxides*; Klimisch, R. L., Larson, J. G., Eds.; Plenum Press: New York, 1975; p 3.
(28) Naccache, C.; Che, M.; Ben Taarit, Y. *Chem. Phys. Lett.* **1972**, *13*, 109.
(29) Chao, C. C.; Lunsford, J. H. *J. Phys. Chem.* **1972**, *76*, 1546.
(30) Yu, J.-S.; Kevan, L. *J. Phys. Chem.* **1994**, *98*, 12436.
(31) Lozos, G. P.; Hoffman, B. M.; Franz, C. G. *QCPE 265*.
(32) Rieger, Ph. H. *J. Magn. Reson*. **1982**, *50*, 485.
(33) Blinder, S. W. *J. Chem. Phys.* **1960,** *33*, 742.
(34) Pilbrow, R. J. In *Transition Ion Electron Paramagnetic Resonance*; Clarendon: Oxford, 1990; p 211.
(35) Press, W. H.; Flannery, B. P.; Teukolsky, S. A.; Vetterling, W. T. In *Numerical Recipes*; Cambridge University Press: Cambridge, 1989; p 289.
(36) Subroutine MINA: Jones, R. E., Sandia Fortran Library.
(37) Herman, R. G. *Inorg. Nucl. Chem. Lett.* **1978**, *14*, 325.
(38) Anpo, M. In *Photochemical Conversion and Storage of Solar Energy*; Pelizzetti, E., Schiavello, M., Eds.; Kluwer: Dordrecht, 1991; p 307.
(39) Anpo, M.; Nomura, T.; Kitao, T.; Giamello, E.; Murphy, D.; Che, M.; Fox, M. A. *Res. Chem. Intermed*. **1991**, *15*, 225.
(40) Spoto, G.; Bordiga, S.; Ricchiardi, G.; Scarano, D.; Zecchina, A.; Geobaldo, F. *J. Chem. Soc., Faraday Trans*. **1995**, *91*, 3285.
(41) Sojka, Z. *Catal. Rev. Sci. Eng*. **1995**, *37*, 61.
(42) Smith, T. D.; Pilbrow, J. R. *Coord. Chem. Rev.* **1981**, *39*, 295.
(43) DeGray, J. A.; Rieger, Ph. H. *Bull. Magn. Reson*. **1987**, *8*, 95.
(44) Lunsford, J. H. *J. Catal*. **1969,** *14*, 379.
(45) Primet, M.; Che, M.; Naccache, C.; Mathieu, M. V.; Imelik, B. *J. Chim. Phys. Phys.-Chim. Biol*. **1970**, *67*, 1629.
(46) Lunsford, J. H. *J. Phys. Chem.* **1968**, *72*, 2141.
(47) Schoonheydt, R. A. *Catal. Rev. Sci. Eng*. **1993**, *35*, 129.
(48) Slinkin, A. A.; Kucherov, A. V.; Chuvylkin, N. D.; Korsunov, V. A.; Kliachko, A. L.; Nikishenko, S. B. *J. Chem. Soc., Faraday Trans*. *1* **1989**, *85*, 3233.
(49) Grünert, W.; Hayes, N. W.; Joyner, R. W.; Shpiro, E. S.; Rafiq, M.; Siddiqui, H.; Baeva, G. N. *J. Phys. Chem.* **1994**, *98*, 10832.
(50) Larsen, S. C.; Aylor, A.; Bell, A. T.; Reimer, J. A. *J. Phys. Chem.* **1994**, *98*, 11533.
(51) Sass, C. E.; Kevan, L. *J. Phys. Chem.* **1989**, *93*, 7856.
(52) Anderson, M. W.; Kevan, L. *J. Phys. Chem.* **1987**, *91*, 4174.
(53) Kucherov, A. V.; Slinkin, A. A. *Zeolites* **1986**, *6*, 175.
(54) Dedecek, J.; Wichterlova, B. *J. Phys. Chem.* **1994**, *98*, 5721.
(55) Trout, B. L.; Chakraborty, A. K.; Bell, A. T. *J. Phys. Chem.* **1996**, *100*, 4173.
(56) Miyamoto, A.; Himei, H.; Oka, Y.; Maruya, E.; Katagiri, M.; Vetrivel, R.; Kubo, M. *Catal. Today* **1994**, *22*, 87.
(57) Enemark, J. H.; Feltham, R. D. *Coord. Chem. Rev*. **1974**, *13*, 339.
(58) Goodman, B. A.; Raynor, J. B. *Adv. Inorg. Chem. Radiochem*. **1970**, *13*, 135.
(59) Sojka, Z.; Giamello, E.; Che, M.; Zecchina, A.; Dyrek, K. *J. Phys. Chem.* **1988**, *92*, 1541.
(60) Garvey, B. R. *J. Phys .Chem.* **1967**, *71*, 51.
(61) Peake, B. M.; Rieger, Ph. H.; Robinson, B. H.; Simpson, J. *J. Am. Chem. Soc.* **1980,** *102*, 156.
(62) Morton, J. R.; Preston, K. F. *J. Magn. Reson*. **1978**, *30*, 577.
(63) Hoffmann, S. K.; Goslar, J.; Osman, M. *Acta Phys. Pol*. **1986**, *A70*, 43.
(64) Pike, R. D.; Rieger, A. L.; Rieger, Ph. H. *J. Chem. Soc., Faraday Trans. 1* **1989**, *85*, 3913.
(65) Atkins, P. W.; Symons, M. C. R. *The Structure of Inorganic Radicals*; Elsevier: Amsterdam, 1967.
(66) Geiger, W. E.; Rieger, Ph. H.; Tulyathan, B.; Rausch, M. D. *J. Am. Chem. Soc.* **1984**, *106*, 7000.
(67) Bower, H. J.; Symons, M. C. R.; Tinling, D. J. A. In *Radical Ions*; Kaiser, E. T., Kevan, L., Eds.; Interscience: New York, 1968.
(68) Hunter, T. F.; Symons, M. C. R. *J. Chem. Soc. A* **1967**, 1770.
(69) Pearson R. G. *Symmetry Rules for Chemical Reactions*; Wiley: New York, 1979.
(70) Nakamoto, K. *Infrared and Raman Spectra of Inorganic and Coordination Compounds*; Wiley: New York, 1986.
(71) Bersuker, I. B. *Kinet. Katal.* **1977**, *18*, 1268.
(72) Bersuker, I. B.; Budnikov, S. S.; Dimoglo, A. S. *Kinet. Katal.* **1982**, *23*, 1454.
(73) Jolly, W. L. *The Inorganic Chemistry of Nitrogen*; Benjamin Inc.: New York, 1964.